European Journal of Neuroscience, Vol. 49, pp. 948–956, 2019 doi:10.1111/ejn.13986

Heterogeneity of retinogeniculate axon arbors

Y. Kate Hong,[1,2,*] Eliza F. Burr,[1] Joshua R. Sanes[2] and Chinfei Chen[1]
[1]F.M. Kirby Neurobiology Center, Department of Neurology, Boston Children's Hospital, Harvard Medical School, Boston, Massachusetts
[2]Department of Molecular and Cellular Biology, Center for Brain Science, Harvard University, Cambridge, Massachusetts

Keywords: direction selective RGC, hidden lamina, lateral geniculate nucleus, retinal ganglion cells

Abstract

The retinogeniculate synapse transmits information from retinal ganglion cells (RGC) in the eye to thalamocortical relay neurons in the visual thalamus, the dorsal lateral geniculate nucleus (dLGN). Studies in mice have identified genetic markers for distinct classes of RGCs encoding different features of the visual space, facilitating the dissection of RGC subtype-specific physiology and anatomy. In this study, we examine the morphological properties of axon arbors of the BD-RGC class of ON-OFF direction selective cells that, by definition, exhibit a stereotypic dendritic arbor and termination pattern in the retina. We find that axon arbors from the same class of RGCs exhibit variations in their structure based on their target region of the dLGN. Our findings suggest that target regions may influence the morphologic and synaptic properties of their afferent inputs.

Introduction

Ray Guillery, a pioneer in the field of Neuroscience, was a strong advocate for interrogating the brain by detailed characterization of its structural organization. He understood that the beautiful shapes of neurons, particularly their elaborate dendritic and axon arbors, can tell us much about the roles they play. For much of his career, he focused on the development and the organization of circuits in the visual system, and especially the thalamus. As our laboratories study this very subject, his papers were required reading for anyone joining our group. In particular, his EM descriptions of glutamatergic and GABAergic synapses in the visual thalamus and descriptions of the glomerular structures are ones that we refer to over and over (Guillery, 1969). Guillery's studies on the lateral geniculate described the "cytoarchitectonic subdivisions" of the nucleus and their relationship to retinal maps. He was interested in all species, whether it be human, cat, ferret, rabbit, mink, squirrel or rat (Colonnier & Guillery, 1964; Guillery, 1966, 1967; Guillery & Kaas, 1974; Guillery, Oberdorfer, & Murphy, 1979; Hickey & Guillery, 1979; Holcombe & Guillery, 1984; Linden, Guillery, & Cucchiaro, 1981; Montero & Guillery, 1968). As a self-proclaimed "descriptive anatomist," Guillery was a strong believer in observational science, generating hypotheses about neural function based on a detailed knowledge of its structure. His papers were engaging, scholarly and refreshingly sincere, pointing out potential caveats to the interpretation based on the available evidence. We pored over his studies describing the terminal patterns of RGC axons as we explored the relationship of axon arbor morphology and functional refinement of the retinogeniculate synapse. Here, in this set of tributes to Guillery, we offer some observations on variability within a specific set of retinogeniculate axons.

In contrast to other species, there is no obvious laminar structure in the rodent dLGN. Yet, a substantial body of evidence gathered over many years points to more organization in the rodent dLGN than suggested by cytoarchitecture alone (Lund, Lund, & Wise, 1974; Martin, 1986). Most notably, two functionally distinct regions, the shell and core, have been described that each contain a retinotopic map, receive inputs from RGCs of distinct morphology, and project to different regions of the visual cortex (Cruz-Martín et al., 2014). In mice, retinal ganglion cells have been extensively analyzed and classified based on their morphology, gene expression and electrophysiological properties (Kay et al., 2011; Kim, Zhang, Meister, & Sanes, 2010), as well as by combining calcium imaging or genetics with computational classification (Baden et al., 2016; Sanes & Masland, 2015; Sümbül et al., 2014). The termination patterns of different RGC classes exhibit distinct patterns in the dLGN. For example, a number of RGCs have a higher propensity to terminate in either the shell or the core region of the nucleus (Cruz-Martín et al., 2014; Huberman et al., 2008, 2009; Kay et al., 2011; Kim et al., 2010; Martersteck et al., 2017; Rivlin-Etzion et al., 2011). For recent reviews on this subject, see: (Dhande & Huberman, 2014; Hong & Chen, 2011; Kerschensteiner & Guido, 2017; Monavarfeshani, Sabbagh, & Fox, 2017).

Here, in the same spirit as Guillery, we present our observations of axon terminal morphologies in the mouse retinogeniculate system,

Correspondence: Chinfei Chen, as above. Email: chinfei.chen@childrens.harvard.edu

*Present address: Department of Neuroscience, Mortimer Zuckerman Mind Brain Behavior Institute, Kavli Institute for Brain Science, Columbia University, New York, NY, USA

Received 25 January 2018, revised 10 May 2018, accepted 23 May 2018

Edited by Paul Bolam. Reviewed by Bart Borghuis, School of Medicine University of Louisville, USA; and Mrinalini Hoon, University of Washington Department of Biological Structure, Biological Structure, USA.

All peer review communications can be found with the online version of the article.

and speculate on what our findings may reveal about the organization of the visual thalamus. We ask whether axon arbors from the same class of RGCs exhibit stereotypic features or whether they vary according to the region of the dLGN that they innervate. In order to address this question, we revisit a previously collected single arbor data set from the FSTL4-CreER mouse line (Hong et al., 2014) that expresses an inducible Cre recombinase in a class of ON-OFF bistratified direction-selective retinal ganglion cells (BD-RGCs) that respond to ventral motion (Kay et al., 2011; Kim et al., 2010). Previously, we used this line to assess the relationship between axon arbor structure and function, limiting our analysis to the region of the dLGN where we obtain our slice electrophysiological recordings of the retinogeniculate synapse (the dorsocaudal region). Here, we catalog the full set of reconstructed arbors to include other regions of the dLGN. We find that axon arbors from the BD-RGC class of neurons exhibit heterogeneous morphology across the dLGN.

Methods

Transgenic animals

All animal procedures were in compliance with the NIH Guide for the Care and Use of Laboratory Animals and approved by the Institutional Animal and Care and Use Committee (IACUC) at Harvard University and Boston Children's Hospital. BD-RGC axon arbors in the dLGN were labeled by crossing FSTL4-CreERT2 mice (Kay et al., 2011; Kim et al., 2010) with Thy1-STOP-YFP line #15 (Buffelli et al., 2003) and analyzed as previously described (Hong et al., 2014). Mice were subcutaneously injected at P0-10 with low doses of tamoxifen (1.5–4 mg/kg) to obtain sparse RGC labeling, or with a high dose (100 mg/kg) for dense labeling. To assess bouton area density, we used the Hb9-GFP transgenic line (Trenholm, Johnson, Li, Smith, & Awatramani, 2011), which densely labels the same population of BD-RGCs (Sanes & Masland, 2015; Trenholm, Johnson, Li, Smith, & Awatramani, 2013).

Histology

Tissue processing, axon imaging, tracing and analysis have been described in detail in supplemental methods in Hong et al. (2014). Briefly, at P30, the mice were anesthesized with Avertin or pentobarbital (100 mg/kg) by intraperitoneal injection and transcardially perfused with 0.1 M phosphate buffered saline followed by 4% w/v paraformaldehyde in PBS. Post-fixed retinae were immunostained against anti-GFP (rabbit; 1:2,000; Millipore), followed by secondary antibody to amplify the GFP (donkey anti-rabbit Alexa-488; Invitrogen). In cases where more than 1 RGC was labeled in the retina, selection of arbors was based on unambiguous identification of retinotopically distant RGCs. This ensured that axon terminals were also separated within the dLGN. Dissected brains were vibratome-sectioned in the sagittal plane at 100 μm, and imaged with confocal microscopy (Zeiss LSM 700 or LSM 710, Figure 1c–e).

Image processing and quantification

For axons spanning multiple sections, confocal image stacks were registered using Imaris Autoaligner (Bitplane) and concatenated to reconstruct the entire arbor, and semi-automatically traced using the Simple Neurite Tracer ImageJ plugin. Traced neurons were imported into Imaris for quantification of the following axon paramaters: total arbor length, number of branch points and segments. Primary and secondary branches of the axons were not included in the total arbor length as they often extended up to 100 μm in length and did not contain boutons. The volume of the arbor was calculated as the 3-D convex hull of the bouton locations. Axon density was quantified as the ratio of length/volume (axon density) of the arbor. Bouton location and number for individual axons was quantified (Imaris, Bitplane) with the restriction that varicosities had to be twice the diameter of the surrounding axon segment (~10 μm on either side). All data sets exhibit normal distribution and we used the student *t* test to assess statistical significance in arbor length and complexity, defined here as the number of branch points and number of segments of the arbor, between different regions of the dLGN.

Boutons were imaged in HB9-GFP animals with a 63× objective (1.4NA; Zeiss, LSM710). Bouton density was defined here as the percent area that GFP expression is present in sample region of interests (ROIs) from dorsal and ventrolateral sections, respectively. Z-stack images (72 × 72 μm^2) were generated using ImageJ, and maximum intensity projection images (0.13 μm optical section) were subsequently analyzed as ROIs using custom routines written in Matlab (Mathworks). ROIs were thresholded with a pixel intensity twice that of each ROI's background and then further processed using erosion and dilation techniques to ensure that primarily boutons, and not corresponding axonal processes, were analyzed. Finally, the total of GFP expression was quantified by analyzing the percent of pixels above threshold relative to the total number of pixels for a given ROI.

To register each axon location to the dLGN template (Figure 1g), epifluorescence or confocal images of DAPI and YFP labeled section were taken at 4×/0.2 NA magnification (Nikon 80i, or 10X/0.3 NA Zeiss LSM 700). The position of the arbor within the dLGN was marked by drawing a contour around the dLGN based on the visible boundaries from labeling with CTB conjugated to an Alexa dye (Invitrogen), or with DAPI staining of the tissue (e.g., Figure 1c) and drawing an oval around the axon arbor relative to the dLGN boundary. Each 100-μm section was matched to correspond to the most similar section of the dLGN template, starting from the most medial dLGN section. Drawn dLGN contours and circles depicting axon location were each manually fit to the corresponding template by non-rigid transformations (translations, rotations and dilations). When axons spanned multiple sections, the section with the largest area of the arbor was used (Figure 1g). The gray shaded region approximates the shell region and was sketched by translating previously published coronal images to the sagittal plane (Cruz-Martín et al., 2014; Grubb & Thompson, 2004). This approximation is not meant to assign reconstructed arbors to shell versus core regions.

Results

P30 RGC axons arbors were reconstructed by taking advantage of the FSTL4-CreER mouse line, which enables labeling of direction selective, ON-OFF bistratified retinal ganglion cells when crossed to a reporter line (Thy1-stop-YFP). Over 90% of these RGCs, called BD-RGCs, respond preferentially to ventral motion (Kay et al., 2011). High doses of tamoxifen densely label BD-RGCs in the retina (Figure 1a,b) and their axon terminals in dLGN (Figure 1c). This class is more frequently found in the dorsal retina when compared to the ventral aspects of the retina (Kim et al., 2010; Figure 1a). By titrating the dose of tamoxifen administered, we were able to achieve sparse labeling of 1–3 retinal ganglion cells in each mouse as previously described (Methods, Hong et al., 2014).

All reconstructed axons terminated in the contralateral zone of the dLGN (Figure 1e,g). We reconstructed arbors in the sagittal plane because we found that fewer sections were necessary to capture the entire BD-RGC arbors when compared to coronal sections of the

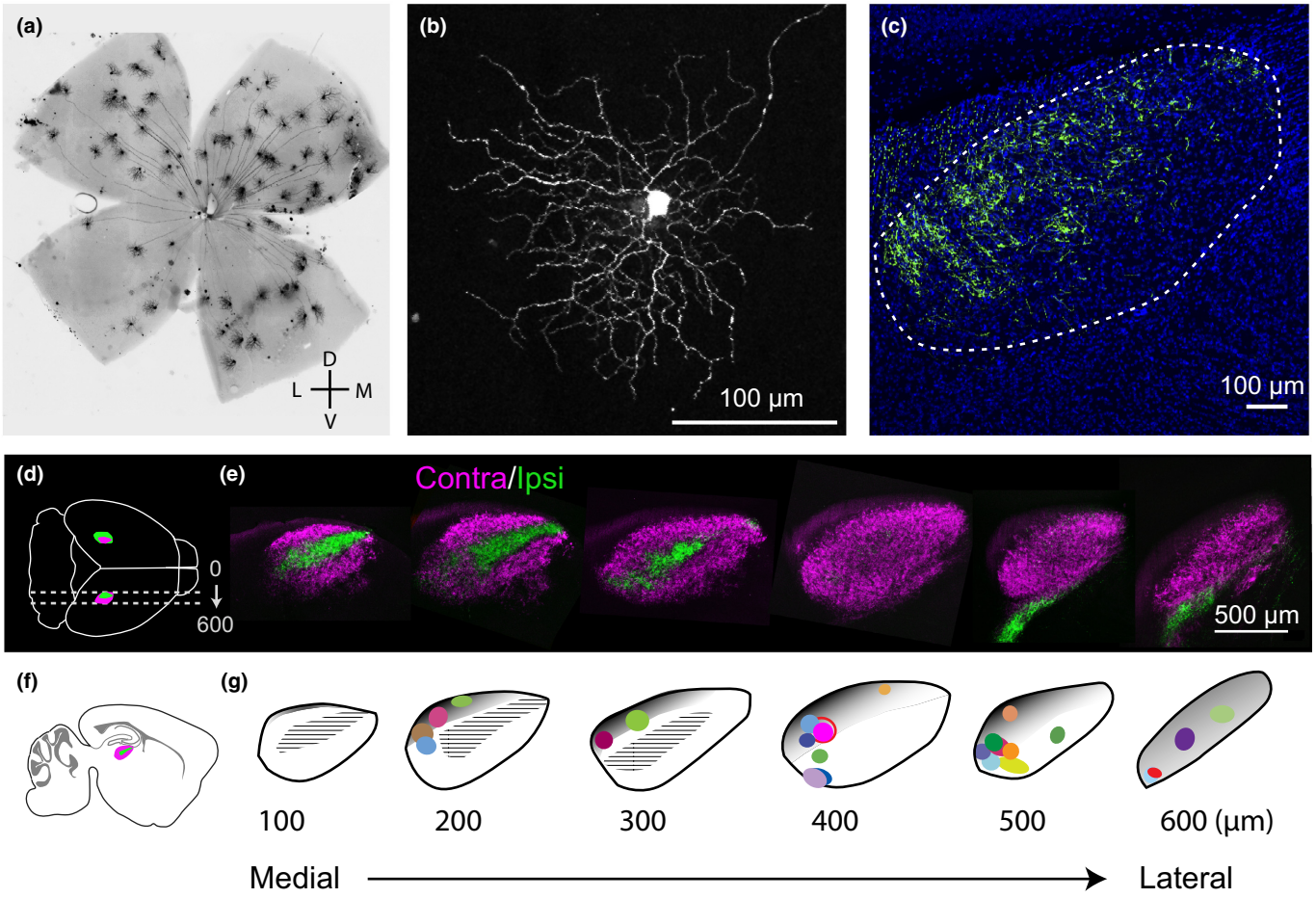

FIG. 1. BD-RGCs axon terminal locations throughout the dLGN. (a) Image of densely labeled BD-RGCs in a whole mount retina from the FSTL4-CreERT2 line. Consistent with previous studies, we find that the dorsal retina is more densely labeled than ventral side. (b) Single BD-RGC in the retina. For single-cell reconstructions, low-dose tamoxifen was used to label just one or a few cells to ensure isolated arbors. (c) dLGN from a mouse with densely labeled BD-RGCs. Axons are found predominantly in the dorsal-caudal region of the nucleus. (d) Schematic of dorsal view of sagittal sections in the intact mouse brain (LGNs in magenta and green). (e) CTB-labeled retinal axon projections delineate contralateral (magenta) and ipsilateral (green) regions within sagittal sections of the dLGN. (f) Schematic of sagittal section with dLGN. (g) dLGN template of individual 100 µm sections from medial to lateral aspects of the dLGN with the location of all 26 reconstructed axons. Each arbor's location is color coded and mapped to the section of the dLGN where it was located. Size and shape of the colored symbols reflect the perimeter of the axon arbor. Gray shaded areas roughly approximate the shell region of the dLGN as previously described in mice for coronal sections (Cruz-Martín et al., 2014; Grubb & Thompson, 2004) and estimated on sections in the sagittal plane. Hatched black regions represent the ipsilateral zone as shown in green in panel e. The distinction between shell and core remains poorly defined at the rostral end. Panels c and e are modified from (Hong et al., 2014).

same thickness. This orientation preference suggests that, at least for BD-RGCs, axon arbors are more likely to expand in the rostral-caudal rather than the medio-lateral direction. This observation is consistent with the idea that an arbor from a given RGC remains in the same retinotopic space in the dLGN (Discussion, Piscopo, El-Danaf, Huberman, & Niell, 2013). Figure 1d,f illustrates sagittal sections obtained from an adult mouse injected with different fluorescence labels (CTB conjugated to Alexa 488 or 647) in each eye. The region of the dLGN receiving ipsilateral retinal projections is found in the first 300 µm from the medial border (green), and extends along the long axis between the anterior and posterior aspects of the nucleus (Figure 1e). Figure 1g maps the location of 26 reconstructed arbors from P30 mice onto the contours of six serial sagittal sections through the dLGN (100 µm, from medial [left] to lateral [right]). In Figures 2 and 3, each arbor's location within the dLGN is paired with the sagittal section template.

Reconstruction of single BD-RGC arbors

Figure 2a–c illustrates the arbors found in the region where we routinely perform electrophysiological recordings. The dorsal-caudal region of the dLGN is where we find the highest incidence of preserved retinal projections, allowing consistent and reliable activation of retinogeniculate EPSCs by optic tract stimulation. Approximately

FIG. 2. Reconstructed BD-RGC axon arbors located in the dorsal dLGN. (a) Schematic of a 2-dimensional projection of the location of 14 axon arbors reconstructed in the dorsocaudal region of the dLGN. Arbor locations from the individual sagittal sections shown in B are collapsed into a single plane. (b) Location of each axon within the sagittal dLGN section template. (c) Reconstructed axon terminals corresponding to the mapped locations in b (*i–iv*). Each axon is color-coded to the corresponding location in a and b. The following arbors were published in a previous study (Hong et al., 2014): arbor c*ii* (left), and the skeletons of arbors c*iii* (first and fourth), c*iv* (first and second). (d-f) RGCs projecting to dorsal anterior dLGN.

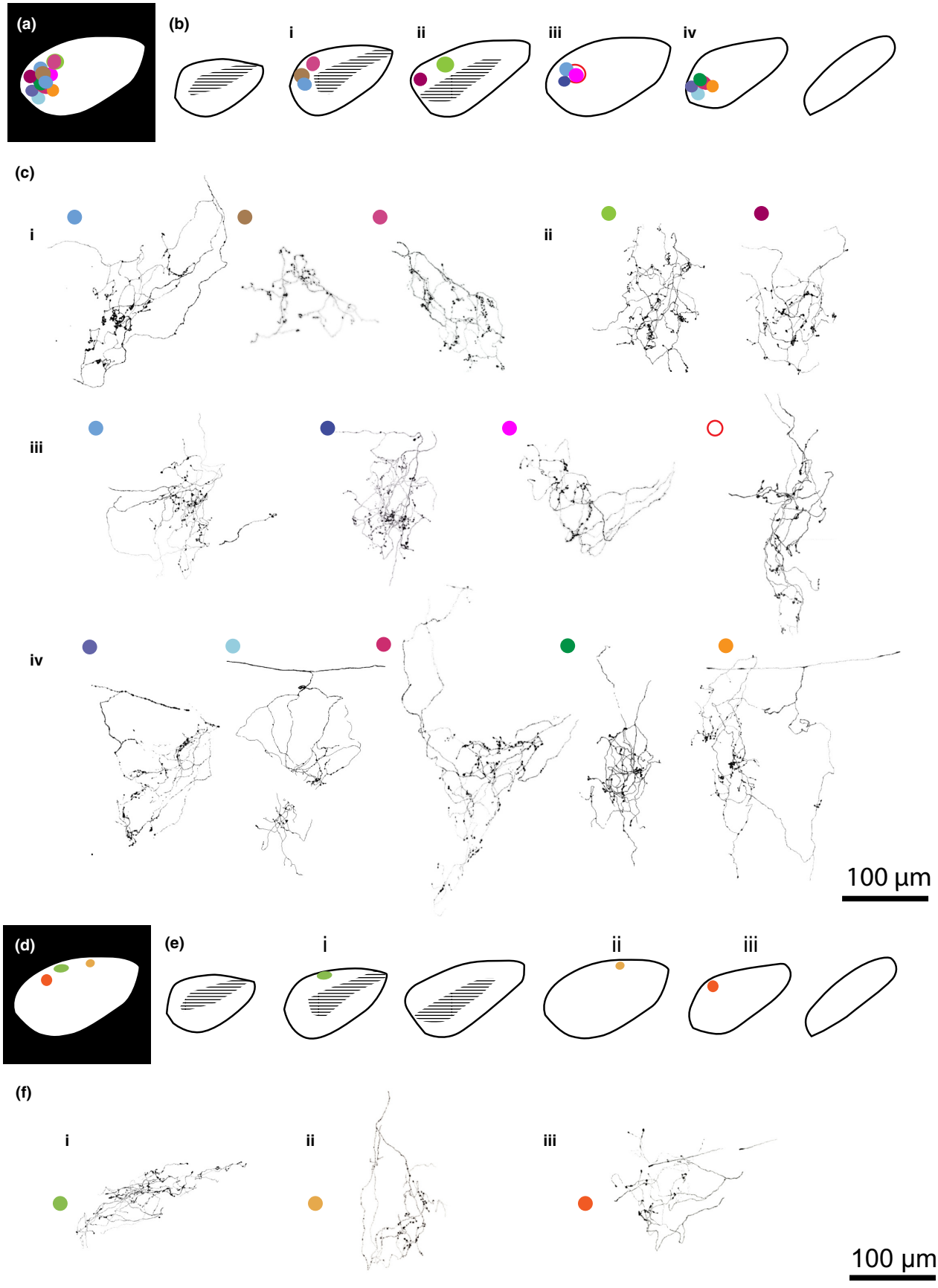

half of the labeled BD-RGC arbors terminated in this region (14/26). As we have previously reported, these arbors are characterized by their large volume, spanning 100–200 μm in their longest axis, their complex branching and prominent boutons that appear to cluster along certain segments of the arbor (Hong et al., 2014).

We add to the study three BD-RGC axons that were found in the dorsal-anterior region of the dLGN (Figure 2d–f), and nine arbors found in the ventrolateral dLGN (Figure 3). The three arbors in dorsal anterior region appeared smaller than the other reconstructed arbors, although the sample size was too small to validate this qualitative impression. Interestingly, the anterior region of the dLGN corresponds retinotopically to the ventral aspect of the retina, where there are far fewer BD-RGC's (Figure 1, Pfeiffenberger, Yamada, & Feldheim, 2006; Kim et al., 2010). The nine arbors in the ventrolateral dLGN were located in the area lateral to the ipsilateral zone (Figure 3b). Many of the arbors in this region demonstrated an elongated morphology (Figure 3c*i*, left and middle; c*ii*, left; *iii* left two arbors).

Axon arbor morphology varies throughout the dLGN

We compared the morphology of BD-RGCs terminating in the dorsal region (Figure 2, combining the dorsal caudal and dorsal anterior regions) to those in the ventrolateral (VL) portion of the dLGN (Figure 3). Axons terminating in VL dLGN were larger than those in the dorsal dLGN, as measured by total axon length (total length: 2.3 ± 0.1 vs. 3.1 ± 0.3 mm, $p = 0.013$). Axon complexity, defined here by number of branch points and segments was also significantly greater for arbors in the VL area when compared to the dorsal dLGN (Figure 4a–c; # branch points: 48.5 ± 4.6 versus 75.8 ± 10.0 $p = 0.009$; # segments: 95.9 ± 8.8 versus 148.3 ± 58.9, $p = 0.009$, student t test for dorsal and VL dLGN-terminating arbors, $n = 17$ versus 9 arbors, respectively, mean ± *SEM*). However, axon density, defined as the ratio of length/volume of the arbor, was not significantly different between the two regions (Figure 4d; 0.009 ± 0.001 vs. 0.007 ± 0.001 μm^{-2}). Thus axon

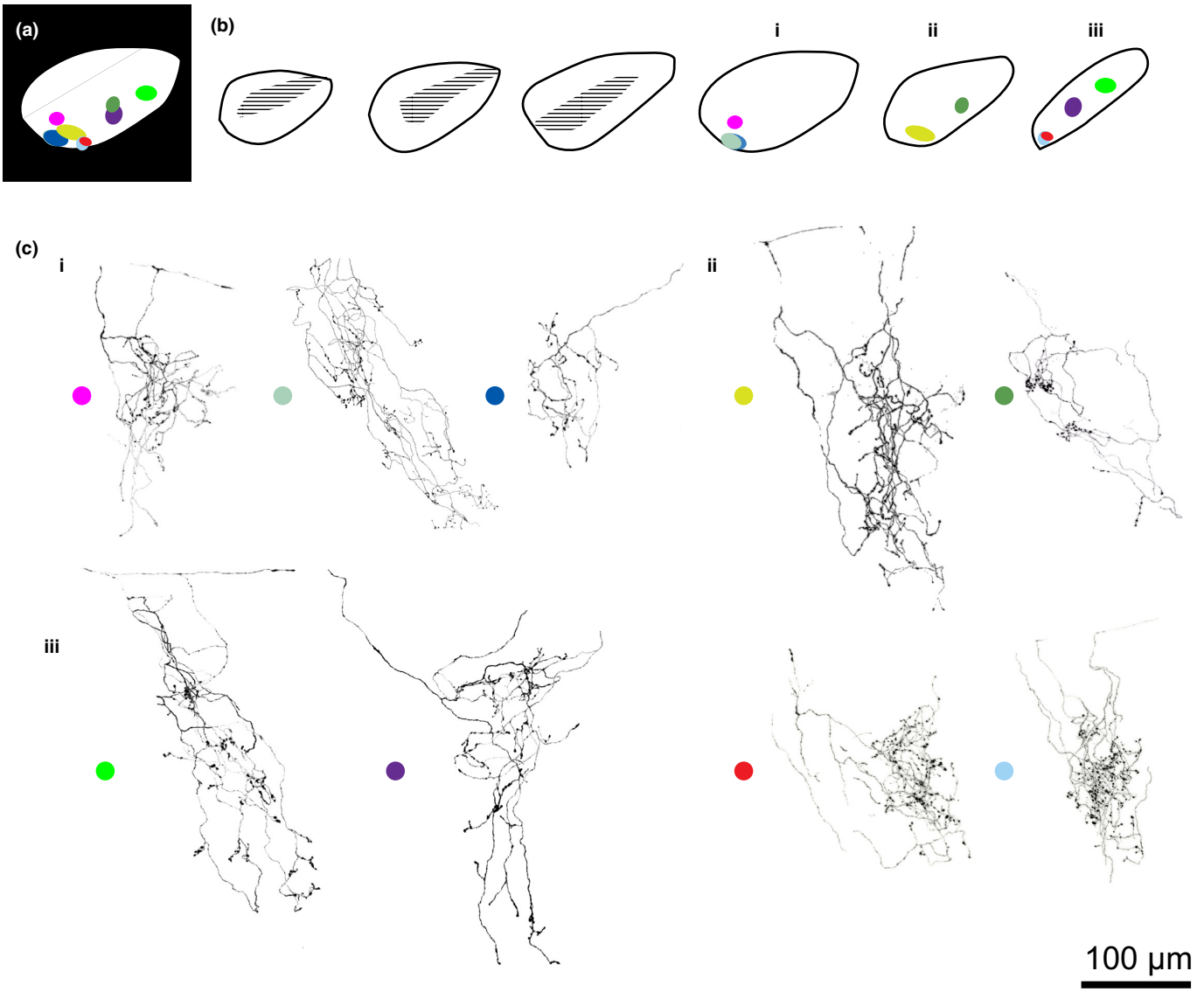

FIG. 3. Reconstructed BD-RGC axon arbors located in the ventrolateral dLGN. (a) Location of 9 axon arbors located in the ventrolateral dLGN. (b) Location of each axon along the sagittal dLGN section template. (c) Reconstructed axon terminals corresponding to each location depicted in b. Schematics are arranged similar to that of Figure 2.

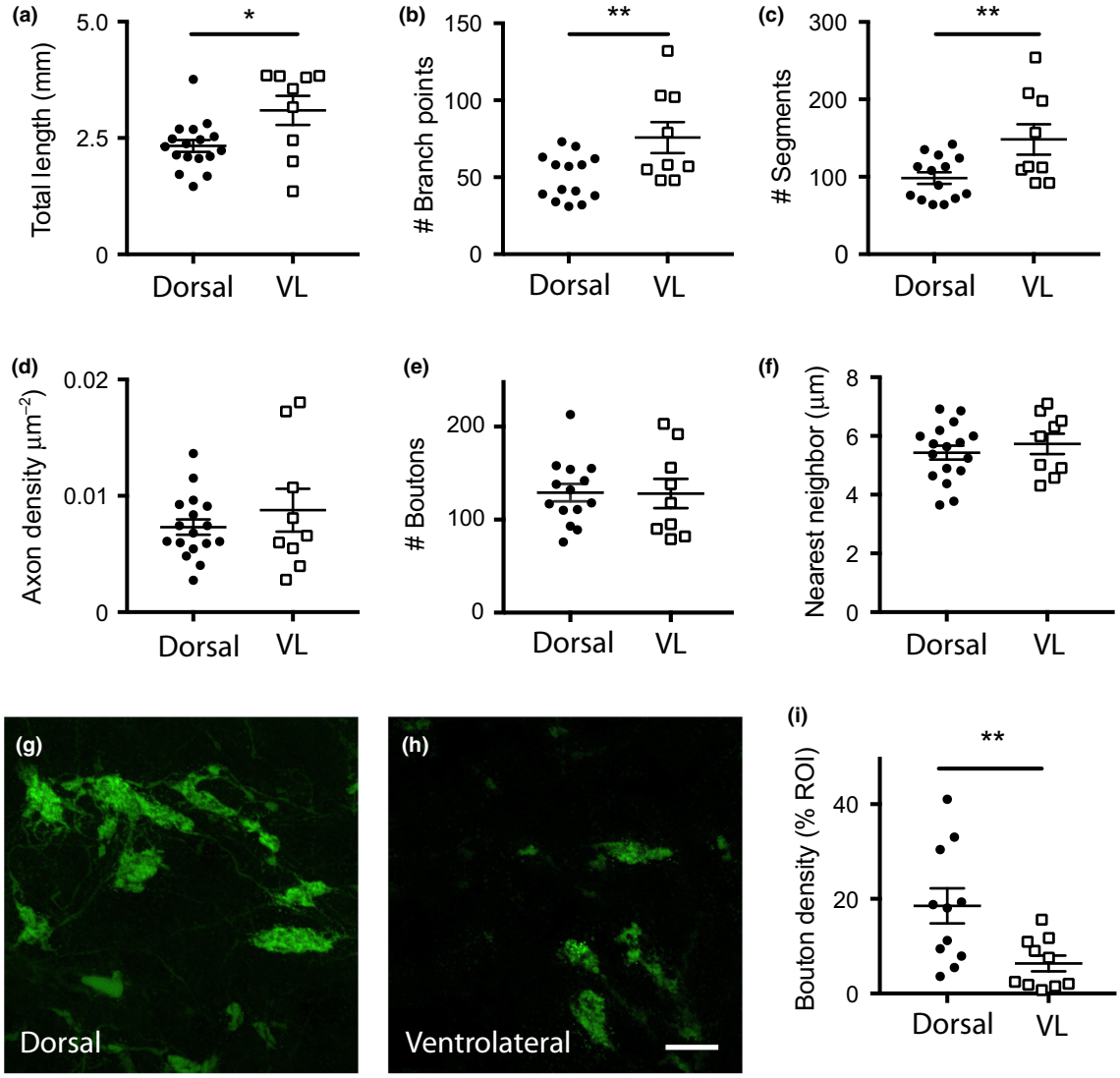

FIG. 4. Quantification of single axon arbor morphology across dLGN. The average properties of BD-RGC axon arbors in the dorsal (dorsal caudal and dorsal anterior arbors in Figure 2) versus ventrolateral (VL) region (in Figure 3) are shown for: (a) total length; (b) # branch points; (c) # segments, (d) axon density, (e) Bouton #, (f) bouton nearest neighbor distance. (g–i) Analysis of total bouton density of BD-RGC axons in densely labeled Hb9-GFP mice. Representative confocal images from the dorsal (g) and ventrolateral (h) regions of the dLGN and quantification of bouton density measured as the % area of the GFP-labeled boutons (i). All data sets were normally distributed based on the D'Agostino & Pearson normality test and analyzed using the student *t* test. $*p < 0.05$., $**p < 0.01$. Lines indicated mean ± *SEM*. Scale bar (g,h): 10 µm.

complexity of RGCs of the same type differs depending on their target region in the dLGN.

Bouton properties of BD-RGC arbors in the dLGN

We next asked whether bouton properties varied between arbors targeting the two dLGN regions. Boutons were defined as varicosities that were greater than twice the nearby axon diameter (Hong et al., 2014). We found that bouton number was not significantly different between dorsal and VL arbors (Figure 4e; 120.1 ± 41.7 vs. 128.1 ± 47.1, boutons/axon, respectively, mean ± *SEM*). Moreover, the nearest neighbor distances between individual boutons were also similar (Figure 4f; 5.43 ± 0.24 vs. 5.73 ± 35 µm for dorsal and VL regions, respectively), suggesting that the degree of bouton clustering within a given arbor did not differ between regions.

Our findings that BD-RGC axons targeting the ventrolateral portion of the LGN are longer and more complex but have equal numbers of boutons as dorsally targeting axons raised the question of whether BD-RGC contribute fewer boutons to the ventrolateral when compared to the dorsal LGN. Due to the fact that the FSTL4-CreER expression is tamoxifen dose-dependent and likely does not label all BD-RGCs, we took advantage of the Hb9-GFP mouse line which densely and uniformly labels the same BD-RGC subtype to address this question. In order to compare the density of boutons contributed from BD-RGCs in the dorsal versus VL dLGN, we measured the total area of GFP-labeled boutons per unit dLGN area in regions of interest (ROIs, 72 × 72 μm^2) throughout many different sections of the dLGN (Figure 4g,h). This analysis revealed that the density of BD-RGC boutons of axons terminating in the dorsal dLGN is significantly higher than that of arbors terminating in the VL dLGN (Figure 4i; 18.52 ± 3.7% vs. 6.4 ± 1.7% of ROI, respectively; $p < 0.001$, student *t* test, $n = 11$ and 10 ROI from dorsal and ventrolateral regions respectively, imaged from 10 slices of three mice). Therefore, although BD-RGC arbors span both dorsal

and ventral regions of the dLGN, synaptic contacts are more prevalent in the dorsal aspect of the nucleus.

Axon branching

One common feature of BD-RGC arbors, regardless of the target location, is that many have branches emerging from multiple sites along the primary and/or secondary axon, often separated by tens to hundreds of microns. Branches often meander through the dLGN rather than taking the shortest path to their final target (e.g., Figure 1c*iv*, Figure 2c*ii*). These distal branches will often converge, intermingling with the other branches of the same arbor in a common target area of the dLGN. Of the 26 reconstructed axons, 8 could be traced back to the primary axon (Figures 2c*iv*-1,2,3,5; 3c*i*-1, 3c*ii*-1, 3c*iii*-1,4, where arbors are numbered sequentially from left to right). Of these 8 arbors, more than 62% (5/8) had 2 or more secondary branches. All of these secondary branches bifurcated, giving rise to twice the number of tertiary branches. The complex branching from the primary axon of BD-RGC axons is likely generalizable to other classes of RGCs and to other species, as they are similar to RGC arbors randomly labeled in mice (Dhande et al., 2011) as well as to RGC arbors reconstructed in cat (Garraghty, Sur, & Sherman, 1986; Mason, 1982; Sretavan & Shatz, 1986; Sur & Sherman, 1982).

Discussion

In this study, we revisit a set of BD-RGC axon arbors that were previously analyzed for changes in the axon skeleton and bouton distribution over development (Hong et al., 2014). We examined the relationship of the arbor structure to their target region of the dLGN at P30-31. By combining the previously analyzed arbors that were located in the dorsocaudal region of the dLGN (Figure 2a–c) with others from dorsal anterior (Figure 2d–f) and ventrolateral (Figure 3) regions of the nucleus, we were able to collect a set of 26 arbors for inspection. Despite having similar dendritic and somatic morphology in the retina, this class of retinal ganglion cells varied in their axon complexity and bouton density depending on their target region in the dLGN.

BD-RGCs target both shell and core regions of the dLGN

Since its initial description, the boundary between shell and core of the rodent dLGN has been defined in different ways. According to the initial descriptions in rat, the outer shell region is the dorsocaudolateral area of the dLGN from the ventricular surface to the dorsal edge of the ipsilateral patch and receives projections from the contralateral eye and superior colliculus (Reese, 1988). The remaining inner core region occupies the ventrorostral area of the dLGN and can be further separated into two ocular lamina, the smaller receiving inputs from the ipsilateral eye, and the larger from the contralateral eye (Reese, 1988). Based on this description of "hidden laminae" within the dLGN, the majority of the reconstructed BD-RGC arbors would fall in the outer shell. However, in mice, initial description delineated a more restricted shell region based on calbindin staining, which is localized to a narrow dorsolateral strip along the rostral-caudal extent of the nucleus. This lamina lies within 100 μm of the optic tract (Grubb & Thompson, 2004). Subsequently, the shell region was redefined to a larger area extending ~200-μm deep from the ventricular surface based on the terminal zones of specific types of direction selective RGCs (Cruz-Martín et al., 2014). Consistent with previous analysis with densely labeled BD-RGCs, we find that individual BD-RGC axons terminate in both the dorsal and ventrolateral regions of the dLGN spanning both shell and core (Kay et al., 2011). Therefore, BD-RGCs do not behave like other classes of direction selective RGCs which have been shown to terminate largely in the shell (Dhande, Stafford, Lim, & Huberman, 2015; Kerschensteiner & Guido, 2017; Martersteck et al., 2017; Monavarfeshani et al., 2017; Seabrook, Burbridge, Crair, & Huberman, 2017). However, total bouton density is greater in the dorsal when compared to the ventrolateral region, suggesting that functional connections may be greater in the shell.

Relating structure to function

Our findings that the BD-RGC axon arbors are better captured in the sagittal section as opposed to the coronal section is consistent with the azimuth and elevation maps described by in vivo electrophysiology (Piscopo et al., 2013). The spatial organization of retinotopy within the dLGN is a smooth progression from dorsomedial to ventrolateral for elevation and from medial to lateral for azimuth. Therefore, arbors that expand in the sagittal plane would remain in the same retinotopic space. In contrast, fewer arbors had their longest axes in the coronal plane, an orientation that would span multiple retinotopic spaces. Interestingly, we find that the in vitro dLGN slice preparation that yields the largest retinogeniculate EPSCs come from ones sectioned in a parasagittal orientation that maximally preserves the optic tract (5° angle relative to midline, (Turner & Salt, 1998; Chen & Regehr, 2000)). As a single thalamocortical relay neuron can receive up to 20–60 bouton contacts from different branches of the same RGC axon, accurate measurement of single fiber or maximal EPSC amplitude will depend on the optimal preservation of RGC axon arbors (Hamos, Van Horn, Raszkowski, & Sherman, 1987; Morgan, Berger, Wetzel, & Lichtman, 2016).

Previously, our in vitro patch clamp recordings were limited to the dorsal-caudal aspect of the dLGN because this was the region where we were most likely to activate relay neurons with a stimulating electrode positioned more than 600 microns away in the optic tract. Recordings from the ventral or dorsal-anterior aspect of the dLGN were rare because connections were less likely to remain intact in the slice preparation. In the future, using optogenetics, it will be interesting to assess whether functional connectivity is similar throughout all regions of the dLGN. Taken together with previous studies, our observations suggest that developmental refinement of different RGC classes may exhibit distinct regional behavior.

Acknowledgements

This work was supported by NIH R21EY018308 and RO1 EY013613 to C.C., RO1 NS29169 to J.R.S., and F31 NS055488 to Y.K.H. Administrative assistance (to CC) and access to the IDDRC Cellular Imaging Core was supported by NIH PO1HD18655 and U54 HD090255. We thank S. Curtiss for her histological and technical assistance.

Conflict of interest

The authors declare no competing financial interests.

Data accessibility

We plan to share all data from the manuscript once published. Investigators should contact Chinfei.chen@childrens.harvard.edu to request access.

Author contribution

YKH, JRS and CC designed the study, YKH performed the arbor reconstructions and analysis, EB performed experiments analyzing bouton density, YKH, JRS and CC interpreted the results and wrote the manuscript.

Abbreviations

3-D, three dimension; BD-RGC, bistratified direction-selective retinal ganglion cells; CTB, cholera toxin Subunit B; DAPI, 4′,6-diamidino-2-phenylindole; dLGN, dorsal lateral geniculate nucleus; EM, electron microscopy; EPSC, excitatory postsynaptic current; FSTL4-creER, flooistatin like 4-cre recombinase estrogen receptor; GABA, gamma aminobutyric acid; GFP, green fluorescent protein; IACUC, Institutional Animal and Care and Use Committee; LSM, Laser scanning microscope; PBS, phosphate buffered saline; PFA, paraformaldehyde; RGC, retinal ganglion cells; Thy1, thymocyte antigen 1; VL, ventrolateral; YFP, yellow fluorescent protein.

References

Baden, T., Berens, P., Franke, K., Rosón, M. R., Bethge, M., & Euler, T. (2016). The functional diversity of retinal ganglion cells in the mouse. *Nature*, **529**, 345–350.

Buffelli, M., Burgess, R. W., Feng, G., Lobe, C. G., Lichtman, J. W., & Sanes, J. R. (2003). Genetic evidence that relative synaptic efficacy biases the outcome of synaptic competition. *Nature*, **424**, 430–434.

Chen, C., & Regehr, W. G. (2000). Developmental remodelingof the retinogeniculate synapse. *Neuron*, **28**, 955–966.

Colonnier, M., & Guillery, R. W. (1964). Synaptic organization in the lateral geniculate nucleus of the monkey. *Zeitschrift für Zellforschung und Mikroskopische Anatomie*, **62**, 333–355.

Cruz-Martín, A., El-Danaf, R. N., Osakada, F., Sriram, B., Dhande, O. S., Nguyen, P. L., … Huberman, A. D. (2014). A dedicated circuit links direction-selective retinal ganglion cells to the primary visual cortex. *Nature*, **507**, 358–361.

Dhande, O. S., Hua, E. W., Guh, E., Yeh, J., Bhatt, S., Zhang, Y., … Crair, M. C. (2011). Development of single retinofugal axon arbors in normal and 2 knock-out mice. *Journal of Neuroscience*, **31**, 3384–3399.

Dhande, O. S., & Huberman, A. D. (2014). ScienceDirectRetinal ganglion cell maps in the brain: Implications for visual processing. *Current Opinion in Neurobiology*, **24**, 133–142.

Dhande, O. S., Stafford, B. K., Lim, J.-H. A., & Huberman, A. D. (2015). Contributions of retinal ganglion cells to subcortical visual processing and behaviors. *Annual Review of Vision Science*, **1**, 291–328.

Garraghty, P. E., Sur, M., & Sherman, S. M. (1986). Role of competitive interactions in the postnatal development of X and Y retinogeniculate axons. *The Journal of Comparative Neurology*, **251**, 216–239.

Grubb, M. S., & Thompson, I. D. (2004). Biochemical and anatomical subdivision of the dorsal lateral geniculate nucleus in normal mice and in mice lacking the β2 subunit of the nicotinic acetylcholine receptor. *Vision Research*, **44**, 3365–3376.

Guillery, R. W. (1966). A study of Golgi preparations from the dorsal lateral geniculate nucleus of the adult cat. *The Journal of Comparative Neurology*, **128**, 21–50.

Guillery, R. W. (1967). Patterns of fiber degeneration in the dorsal lateral geniculate nucleus of the cat following lesions in the visual cortex. *The Journal of Comparative Neurology*, **130**, 197–221.

Guillery, R. W. (1969). The organization of synaptic interconnections in the laminae of the dorsal lateral geniculate nucleus of the cat. *Zeitschrift für Zellforschung und Mikroskopische Anatomie*, **96**, 1–38.

Guillery, R. W., & Kaas, J. H. (1974). The effects of monocular lid suture upon the development of the lateral geniculate nucleus in squirrels (*Sciureus carolinensis*). *The Journal of Comparative Neurology*, **154**, 433–442.

Guillery, R. W., Oberdorfer, M. D., & Murphy, E. H. (1979). Abnormal retino-geniculate and geniculo-cortical pathways in several genetically distinct color phases of the mink (*Mustela vison*). *The Journal of Comparative Neurology*, **185**, 623–655.

Hamos, J. E., Van Horn, S. C., Raszkowski, D., & Sherman, S. M. (1987). Synaptic circuits involving and individual retinogeniculate axon in cat. *The Journal of Comparative Neurology*, **259**, 165–292.

Hickey, T. L., & Guillery, R. W. (1979). Variability of laminar patterns in the human lateral geniculate nucleus. *The Journal of Comparative Neurology*, **183**, 221–246.

Holcombe, V., & Guillery, R. W. (1984). The organization of retinal maps within the dorsal and ventral lateral geniculate nuclei of the rabbit. *The Journal of Comparative Neurology*, **225**, 469–491.

Hong, Y. K., & Chen, C. (2011). Wiring and rewiring of the retinogeniculate synapse. *Current Opinion in Neurobiology*, **21**, 228–237.

Hong, Y. K., Park, S., Litvina, E. Y., Morales, J., Sanes, J. R., & Chen, C. (2014). Refinement of the retinogeniculate synapse by bouton clustering. *Neuron*, **84**, 332–339.

Huberman, A. D., Manu, M., Koch, S. M., Susman, M. W., Lutz, A. B., Ullian, E. M., … Barres, B. A. (2008). Architecture and activity-mediated refinement of axonal projections from a mosaic of genetically identified retinal ganglion cells. *Neuron*, **59**, 425–438.

Huberman, A. D., Wei, W., Elstrott, J., Stafford, B. K., Feller, M. B., & Barres, B. A. (2009). Genetic identification of an On-Off direction-selective retinal ganglion cell subtype reveals a layer-specific subcortical map of posterior motion. *Neuron*, **62**, 327–334.

Kay, J. N., De la Huerta, I., Kim, I.-J., Zhang, Y., Yamagata, M., Chu, M. W., … Sanes, J. R. (2011). Retinal ganglion cells with distinct directional preferences differ in molecular identity, structure, and central projections. *Journal of Neuroscience*, **31**, 7753–7762.

Kerschensteiner, D., & Guido, W. (2017). Organization of the dorsal lateral geniculate nucleus in the mouse. *Visual Neuroscience*, **34**, E008.

Kim, I. J., Zhang, Y., Meister, M., & Sanes, J. R. (2010). Laminar restriction of retinal ganglion cell dendrites and axons: Subtype-specific developmental patterns revealed with transgenic markers. *Journal of Neuroscience*, **30**, 1452–1462.

Linden, D. C., Guillery, R. W., & Cucchiaro, J. (1981). The dorsal lateral geniculate nucleus of the normal ferret and its postnatal development. *The Journal of Comparative Neurology*, **203**, 189–211.

Lund, R. D., Lund, J. S., & Wise, R. P. (1974). The organization of the retinal projection to the dorsal lateral geniculate nucleus in pigmented and albino rats. *The Journal of Comparative Neurology*, **158**, 383–403.

Martersteck, E. M., Hirokawa, K. E., Evarts, M., Bernard, A., Duan, X., Li, Y., … Harris, J. A. (2017). Diverse central projection patterns of retinal ganglion cells. *Cell Reports*, **18**, 2058–2072.

Martin, P. R. (1986). The projection of different retinal ganglion cell classes to the dorsal lateral geniculate nucleus in the hooded rat. *Experimental Brain Research*, **62**, 77–88.

Mason, C. A. (1982). Development of terminal arbors of retino-geniculate axons in the kitten–I. Light microscopical observations. *Neuroscience*, **7**, 541–559.

Monavarfeshani, A., Sabbagh, U., & Fox, M. A. (2017). Not a one-trick pony: Diverse connectivity and functions of the rodent lateral geniculate complex. *Visual Neuroscience*, **34**, E012.

Montero, V. M., & Guillery, R. W. (1968). Degeneration in the dorsal lateral geniculate nucleus of the rat following interruption of the retinal or cortical connections. *The Journal of Comparative Neurology*, **134**, 211–242.

Morgan, J. L., Berger, D. R., Wetzel, A. W., & Lichtman, J. W. (2016). The fuzzy logic of network connectivity in mouse visual thalamus. *Cell*, **165**, 192–206.

Pfeiffenberger, C., Yamada, J., & Feldheim, D. A. (2006). Ephrin-As and patterned retinal activity act together in the development of topographic maps in the primary visual system. *Journal of Neuroscience*, **26**, 12873–12884.

Piscopo, D. M., El-Danaf, R. N., Huberman, A. D., & Niell, C. M. (2013). Diverse visual features encoded in mouse lateral geniculate nucleus. *Journal of Neuroscience*, **33**, 4642–4656.

Reese, B. E. (1988). "Hidden lamination" in the dorsal lateral geniculate nucleus: The functional organization of this thalamic region in the rat. *Brain Research*, **472**, 119–137.

Rivlin-Etzion, M., Zhou, K., Wei, W., Elstrott, J., Nguyen, P. L., Barres, B. A., … Feller, M. B. (2011). Transgenic mice reveal unexpected diversity of on-off direction-selective retinal ganglion cell subtypes and brain structures involved in motion processing. *Journal of Neuroscience*, **31**, 8760–8769.

Sanes, J. R., & Masland, R. H. (2015). The types of retinal ganglion cells: Current status and implications for neuronal classification. *Annual Review of Neuroscience*, **38**, 221–246.

Seabrook, T. A., Burbridge, T. J., Crair, M. C., & Huberman, A. D. (2017). Architecture, function, and assembly of the mouse visual system. *Annual Review of Neuroscience*, **40**, 499–538.

Sretavan, D. W., & Shatz, C. J. (1986). Prenatal development of retinal ganglion cell axons: Segregation into eye-specific layers within the cat's lateral geniculate nucleus. *Journal of Neuroscience*, **6**, 234–251.

Sümbül, U., Song, S., McCulloch, K., Becker, M., Lin, B., Sanes, J. R., … Seung, H. S. (2014). A genetic and computational approach to structurally classify neuronal types. *Nature Communications*, **5**, 266–47.

Sur, M., & Sherman, S. M. (1982). Retinogeniculate terminations in cats: Morphological differences between X and Y cell axons. *Science (New York, N.Y.)*, **218**, 389–391.

Trenholm, S., Johnson, K., Li, X., Smith, R. G., & Awatramani, G. B. (2011). Parallel mechanisms encode direction in the retina. *Neuron*, **71**, 683–694.

Trenholm, S., Johnson, K., Li, X., Smith, R. G., & Awatramani, G. B. (2013). Parallel mechanisms encode direction in the retina: Erratum. *Neuron*, **77**(1), 204–208.

Turner, J. P., & Salt, T. E. (1998). Characterization of sensory and corticothalamic excitatory inputs to rat thalamocortical neurones in vitro. *The Journal of Physiology*, **510**(Pt 3), 829–843.